

# Topological superconductivity and Majorana fermions in half-metal / superconductor heterostructure

Suk Bum Chung, Hai-Jun Zhang, Xiao-Liang Qi, and Shou-Cheng Zhang

*Department of Physics, Stanford University, Stanford, CA 94305*

(Dated: May 20, 2022)

A half-metal is by definition spin-polarized at its Fermi level and therefore was conventionally thought to have little proximity effect with an *s*-wave superconductor. Here we show that if there is spin-orbit coupling at the interface between a single-band half-metal and an *s*-wave superconductor,  $p_x + ip_y$  superconductivity would be induced on the half-metal. This can give us a topological superconductor with a single chiral Majorana edge state. We show that two atomic layers of  $\text{CrO}_2$  or  $\text{CrTe}$  give us the single-band half-metal and is thus a candidate material for realizing this physics.

*Introduction:* Possibility of Majorana fermions arising out of condensed matter system has aroused great interest in recent years<sup>1</sup>. One class of systems where Majorana fermions can appear is the two-dimensional (2D) chiral superconductor which has a full pairing gap in the bulk, and  $\mathcal{N}$  gapless chiral one-dimensional (1D) states, which consists of Majorana fermions<sup>2,3</sup>, at the edge. When such a chiral topological superconductor (TSC) has  $\mathcal{N} = 1$ , a single Majorana zero mode would be bound to a vortex core<sup>3–5</sup>, giving rise to non-Abelian statistics which can be potentially useful for topological quantum computation<sup>6</sup>. The most straightforward way to realize such chiral TSC is the intrinsic  $p_x + ip_y$  superconductivity in spinless fermions<sup>3</sup>. The strongest candidate material for this superconductivity, albeit a spinful version, is  $\text{Sr}_2\text{RuO}_4$ <sup>7</sup>, but the experimental situation is not definitive<sup>8</sup>. Recently, there has been alternative proposals involving inducing *s*-wave superconductivity in material with strong spin-orbit coupling through proximity effect<sup>9–13</sup>. In this Letter, we show that one can obtain the spin-polarized  $p_x + ip_y$  superconductivity in a half-metal through proximity to the conventional *s*-wave superconductor.

We consider the pair formation on a half-metal (HM) that is in proximity contact to an *s*-wave superconductor (SC). A HM, by definition, is spin-polarized at the Fermi surface<sup>14</sup>, *i.e.* it is a metal for the majority-spin and an insulator for the minority-spin. Our proposal has two major advantages over other current proposals. Firstly, the topological superconductor phase in our approach exists in a wide range of Fermi level. Secondly, we expect the proximity effect between SC and HM to be more robust than that between SC and semiconductor, due to better Fermi surface matching. It has been known that at the normal metal to *s*-wave SC interface, *p*-wave pairing can be induced because inversion symmetry is broken<sup>15</sup>. Eschrig *et al.* showed that when normal metal is HM, even frequency pairing would be mostly *p*-wave<sup>16</sup>. Furthermore, there are experimental indications that strong proximity effect between a HM and an *s*-wave superconductor is possible<sup>17,18</sup>. Here we will show how we can obtain  $p_x + ip_y$  pairing symmetry in a 2D HM when it is coupled to an *s*-wave superconductor only through electron hopping across the interface. If the 2D HM has a sin-

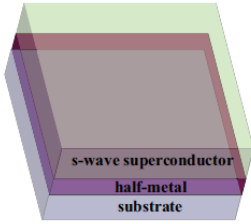


FIG. 1. The heterostructure for obtaining  $p_x + ip_y$  superconductivity. The half-metal layer has a 2D electronic structure with a single Fermi surface without spin degeneracy. It is coupled to the *s*-wave superconductor through hopping. The substrate stabilizes the crystal structure of the half-metal but does not affect qualitatively the half-metal electronic structure.

gle Fermi pocket without spin degeneracy, such  $p_x + ip_y$  pairing will give us the TSC with  $\mathcal{N} = 1$ . We will show band calculation for thin film material that is HM and has a single Fermi pocket. We will also discuss the suitable superconductor for optimizing this proximity effect and the method we can use for detecting the  $p_x + ip_y$  pairing in the HM.

*Basic Model:* We consider the model with a *s*-wave superconductor and a 2D half-metal coupled by a weak hopping between two systems:

$$\mathcal{H} = \mathcal{H}_{SC} + \mathcal{H}_{HM} + \mathcal{H}_t \quad (1)$$

where

$$\begin{aligned} \mathcal{H}_{SC} &= \sum_{\mathbf{k},\sigma} (\epsilon'_{\mathbf{k}} - \mu') c_{\mathbf{k}\sigma}^\dagger c_{\mathbf{k}\sigma} + \sum_{\mathbf{k}} (\Delta'_{\mathbf{k}} c_{\mathbf{k}\uparrow}^\dagger c_{-\mathbf{k}\downarrow}^\dagger + \text{h.c.}), \\ \mathcal{H}_{HM} &= \sum_{\mathbf{k}} (\epsilon_{\mathbf{k}} - \mu) f_{\mathbf{k}\uparrow}^\dagger f_{\mathbf{k}\uparrow}, \\ \mathcal{H}_t &= \sum_{\mathbf{k}\sigma} (t_{\mathbf{k},\uparrow\sigma} f_{\mathbf{k}\uparrow}^\dagger c_{\mathbf{k}\sigma} + \text{h.c.}) \end{aligned} \quad (2)$$

(note  $\mathbf{k}$  is an in-plane vector). While  $\mathcal{H}_t$  requires  $\mathbf{k}$  to be conserved in the hopping process, it does allow for dependence of hopping on  $\mathbf{k}$ . We emphasize that  $\mathcal{H}_t$  also allows for spin-flip hopping.

Within this model, the symmetry of Cooper pairs formed on the half-metal side,  $\langle f_{-\mathbf{k}\uparrow} f_{\mathbf{k}\uparrow} \rangle$ , is determined

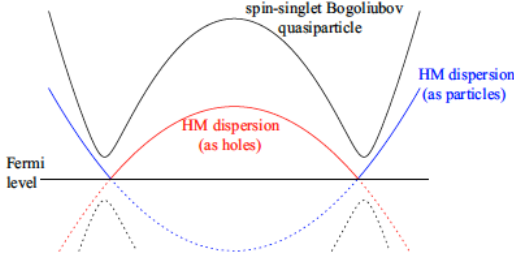


FIG. 2. Schematic representation of the HM and SC band for weak hopping. Two HM bands, with negative energy portions dotted, are due to the artificial doubling of degrees of freedom in the Bogoliubov-de Gennes formalism. In this formalism, the pairing amplitude and gap require hybridization of the ‘particle’ and ‘hole’ bands, which can only occur through hopping to the SC.

entirely by  $t_{\mathbf{k},\uparrow\sigma}$ . In this model, the only channel for this Cooper pair formation is to have the HM electrons with momenta  $\mathbf{k}$  and  $-\mathbf{k}$  hop to the SC side to form a pair there. This process requires that hopping flips the spin of either one, but not both, of the  $\mathbf{k}$  and  $-\mathbf{k}$  electrons. Since the Cooper pair on the SC side is in the spin-singlet  $s$ -wave state, the two spin-flip amplitude interferes destructively, giving us

$$\langle f_{-\mathbf{k}\uparrow} f_{\mathbf{k}\uparrow} \rangle \propto t_{\mathbf{k},\uparrow\uparrow} t_{-\mathbf{k},\uparrow\downarrow} - t_{-\mathbf{k},\uparrow\uparrow} t_{\mathbf{k},\uparrow\downarrow} \quad (3)$$

with an  $s$ -wave multiplicative factor; this gives us odd spatial parity. In the limit of weak hopping,  $|t_{\mathbf{k},\uparrow\sigma}| \ll |\Delta'_{\mathbf{k}}|$ , we find the pairing amplitude at the HM Fermi surface (*i.e.* for  $\mathbf{k}$  that satisfies  $\epsilon_{\mathbf{k}} - \mu = 0$ ) to be (see Appendix A 1 for details)

$$\langle f_{-\mathbf{k}\uparrow} f_{\mathbf{k}\uparrow} \rangle \approx \frac{1}{2} \frac{\eta_{\mathbf{k}}}{\sqrt{|\eta_{\mathbf{k}}|^2 + |\zeta_{\mathbf{k}}|^2}}, \quad (4)$$

where

$$\begin{aligned} \eta_{\mathbf{k}} &= (t_{\mathbf{k},\uparrow\uparrow} t_{-\mathbf{k},\uparrow\downarrow} - t_{\mathbf{k},\uparrow\downarrow} t_{-\mathbf{k},\uparrow\uparrow}) \langle c_{-\mathbf{k}\downarrow} c_{\mathbf{k}\uparrow} \rangle|_{\epsilon_{\mathbf{k}}=\mu}, \\ \zeta_{\mathbf{k}} &= \frac{|t_{\mathbf{k},\uparrow\uparrow}|^2 + |t_{\mathbf{k},\uparrow\downarrow}|^2}{2} \frac{\epsilon'_{\mathbf{k}} - \mu'}{E'_{\mathbf{k}}} \Big|_{\epsilon_{\mathbf{k}}=\mu} \end{aligned} \quad (5)$$

with  $E'_{\mathbf{k}} = \sqrt{(\epsilon'_{\mathbf{k}} - \mu')^2 + |\Delta'_{\mathbf{k}}|^2}$  (we also assume  $|t_{\mathbf{k},\uparrow\sigma}|^2 = |t_{-\mathbf{k},\uparrow\sigma}|^2$ ). One key message from Eqs.(4) and (5) is that we have at the HM Fermi surface  $\langle f_{-\mathbf{k}\uparrow} f_{\mathbf{k}\uparrow} \rangle = e^{i\phi_{\mathbf{k}}} \langle c_{-\mathbf{k}\downarrow} c_{\mathbf{k}\uparrow} \rangle$ , with  $e^{i\phi_{\mathbf{k}}}$  being the phase factor of  $t_{\mathbf{k},\uparrow\uparrow} t_{-\mathbf{k},\uparrow\downarrow} - t_{\mathbf{k},\uparrow\downarrow} t_{-\mathbf{k},\uparrow\uparrow}$ , if the Fermi surfaces of the HM and the SC match exactly (*i.e.*  $\epsilon'_{\mathbf{k}} - \mu' = 0$  when  $\epsilon_{\mathbf{k}} - \mu = 0$ ). Physically,  $\eta_{\mathbf{k}}$  is proportional to the amplitude that the  $\mathbf{k}$  and  $-\mathbf{k}$  HM electrons hop over to the  $s$ -wave SC to form a Cooper pair, while  $\zeta_{\mathbf{k}}$  is proportional to the amplitude that these electrons hop over to the SC with their spin aligned and therefore do not form a Cooper pair.

Our model gives us not only the pairing amplitude but also the pairing gap on the HM side. In the weak hopping

limit we have been discussing,

$$\Delta_{\mathbf{k}}^{HM} = \frac{\eta_{\mathbf{k}}}{E'_{\mathbf{k}}} = \frac{t_{\mathbf{k},\uparrow\uparrow} t_{-\mathbf{k},\uparrow\downarrow} - t_{\mathbf{k},\uparrow\downarrow} t_{-\mathbf{k},\uparrow\uparrow}}{2E'_{\mathbf{k}}} \Delta'_{\mathbf{k}} \quad (6)$$

at the HM Fermi surface, as we will show in Appendix. Note here that  $|\Delta'_{\mathbf{k}}|$  is maximized when we have a perfect Fermi surface matching between the HM and the SC. We point out that since our HM is 2D, proximity to a SC leads to a pairing gap<sup>19,20</sup>. Moreover, since this gap  $\Delta^{HM}$  comes from the HM electron pairing, as we can see from Eqs.(4) and (7), we conclude that the topological property of SC induced in the HM to be determined entirely by  $\Delta^{HM}$ , or equivalently, by  $t_{\mathbf{k},\uparrow\sigma}$ .

In the limit of strong hopping, we obtain a much larger pairing gap while the pairing symmetry is still determined by the hopping as in Eq.(3). Our strong hopping limit requires at the HM Fermi surface  $\epsilon_{\mathbf{k}} - \mu = 0$ , the energetics is dominated by the spin-conserving hopping  $t_{\mathbf{k},\uparrow\uparrow}$ , *i.e.*  $|t_{\mathbf{k},\uparrow\uparrow}| \gg E'_{\mathbf{k}}$  and  $|t_{\mathbf{k},\uparrow\uparrow}| \gg |t_{\mathbf{k},\uparrow\downarrow}|$ . Within this model, at the HM Fermi surface ( $\epsilon_{\mathbf{k}} - \mu = 0$ ), while the pairing amplitude remains that of Eq.(4), the pairing gap at the HM is now given as (see Appendix A 2 for details)

$$\Delta_{\mathbf{k}}^{HM} = \frac{\eta_{\mathbf{k}} E'_{\mathbf{k}}}{|t_{\mathbf{k},\uparrow\uparrow}|^2} = \frac{t_{\mathbf{k},\uparrow\uparrow} t_{-\mathbf{k},\uparrow\downarrow} - t_{\mathbf{k},\uparrow\downarrow} t_{-\mathbf{k},\uparrow\uparrow}}{2|t_{\mathbf{k},\uparrow\uparrow}|^2} \Delta'_{\mathbf{k}}. \quad (7)$$

The HM pairing gap in the strong hopping limit, given in Eq.(7), is much larger than that in the weak hopping limit, given in Eq.(6). This is because in Eq.(7),  $\Delta^{HM}$  is proportional to  $t_{\uparrow\downarrow}/t_{\uparrow\uparrow}$ , while in Eq.(6), it is proportional to  $t_{\uparrow\downarrow} t_{\uparrow\uparrow}/E'^2$ . Similar analysis can be applied to the proximity of HM with a 3D SC, in which case  $\Delta_{\mathbf{k}}^{HM}$  is still linearly proportional to  $t_{\uparrow\downarrow}$ .

*Interface hopping:* To show how this HM / SC proximity effect gives us the  $p_x + ip_y$  pairing, we first discuss the symmetry  $t_{\mathbf{k},\uparrow\sigma}$ . We note that, since inversion symmetry is broken at the HM/SC interface, there will be an interface Rashba spin-orbit coupling (SOC)<sup>15</sup>:

$$\mathcal{H}_{SOC} = \hbar\alpha(\boldsymbol{\sigma} \times \mathbf{k}) \cdot \hat{\mathbf{n}}\delta(\hat{\mathbf{n}} \cdot \mathbf{r}). \quad (8)$$

with  $\hat{\mathbf{n}}$  the normal direction of the interface. To account for this interface SOC in our model Eq.(2), we need to have a hopping term that has the same symmetry as Eq.(8). Such a hopping term, in the momentum space, can be written as

$$\mathcal{H}_{t-SOC} = t_{SOC} \sum_{\mathbf{k}} F_{\mathbf{k}}^{\dagger} (\sigma^x \sin k_y a - \sigma^y \sin k_x a) C_{\mathbf{k}} + \text{h.c.}, \quad (9)$$

where  $F_{\mathbf{k}} = (f_{\mathbf{k}\uparrow}, f_{\mathbf{k}\downarrow})^T$  and  $C_{\mathbf{k}} = (c_{\mathbf{k}\uparrow}, c_{\mathbf{k}\downarrow})^T$ . However, the terms involving  $f_{\mathbf{k}\downarrow}$  can be ignored for the HM/SC interface, as these terms involve process occurring at energy larger than the minority-spin gap of the HM.

We can now show explicitly how we obtain the  $p_x + ip_y$  pairing from  $t_{\mathbf{k},\uparrow\sigma}$ . If we also include the spin-conserving hopping that is momentum-independent, we obtain

$$\begin{aligned} t_{\mathbf{k},\uparrow\uparrow} &= t_0 \\ t_{\mathbf{k},\uparrow\downarrow} &= t_{SOC}(i \sin k_x a + \sin k_y a). \end{aligned} \quad (10)$$

We note that for a square lattice in the real space representation, the spin-conserving hopping of Eq.(10) is ‘vertical’, *i.e.*  $t_0 \sum_i f_{i\uparrow}^\dagger c_{i\uparrow} + \text{h.c.}$ , while the spin-flip hopping is of the ‘nearest neighbor’ type, *i.e.*  $t_{SO} \sum_{(ij)} \exp[i\theta_{ij}] f_{i\uparrow}^\dagger c_{j\downarrow} + \text{h.c.}$ , where  $\theta_{ij}$  gives the chiral  $p$ -wave symmetry. Inserting these  $t_{\mathbf{k},\uparrow\sigma}$  into Eq.(3) gives us the chiral  $p$ -wave pairing on the HM side:

$$\begin{aligned} \langle f_{-\mathbf{k}\uparrow} f_{\mathbf{k}\uparrow} \rangle &\propto t_{\mathbf{k},\uparrow\uparrow} t_{-\mathbf{k},\uparrow\downarrow} - t_{-\mathbf{k},\uparrow\uparrow} t_{\mathbf{k},\uparrow\downarrow} \\ &= -2it_0 t_{SOC} (\sin k_x a - i \sin k_y a). \end{aligned} \quad (11)$$

Eq.(10) gives us the  $\mathcal{N} = 1$  TSC in the strong hopping limit as well as the weak hopping limit (see Appendix A 2 for details). We also note that the chiral  $p$ -wave is mentioned as the likely pairing symmetry if there is intrinsic SC in a HM<sup>21</sup>.

From the origin of the interface SOC, we can estimate of the HM pairing gap to be  $|\Delta^{HM}| \sim |\Delta'|(\alpha_{SOC}/W)$ , where  $\alpha_{SOC}$  is the Rashba SOC of the  $s$ -wave SC and  $W$  is the bandwidth. Physically, when SOC is strong for the  $s$ -wave SC but weak for the HM, we can expect to have the interface SOC. This situation is experimentally relevant because  $s$ -wave SC can exist in materials with strong SOC, while the spin-polarized ARPES indicates complete spin polarization for the HM, as in  $\text{CrO}_2$ <sup>22</sup>. Assuming that we have zero effective SOC on the HM, we will effectively have the spin-orbit coupling hopping  $t_{SOC} \sim (\alpha_{SOC}/W)t_0$  induced through second order perturbation. This is sufficient for estimating  $|\Delta^{HM}|$ , because, in the strong hopping limit, we find  $\Delta^{HM} \sim (t_{SOC}/t_0)\Delta'$  by inserting Eq.(11) into Eq.(7).

We also point out that this HM/SC proximity effect can provide us with a means to obtain a multi-domain chiral  $p$ -wave SC. Eqs.(9) and (10) show us that if we reverse the HM spin polarization, than we will also reverse the chirality of the induced SC. Therefore in a HM, a domain boundary between opposite spin polarization will also be the domain boundary between the  $p+ip$  and  $p-ip$  domain when SC is induced.

*Candidate material:* We note that although the spin-polarized (or single-spin)  $p_x + ip_y$  SC with a single Fermi pocket gives us the  $\mathcal{N} = 1$  TSC<sup>3</sup>, the same may not be said for the  $p_x + ip_y$  SC with multiple Fermi pockets<sup>23,24</sup>. Therefore to obtain the  $\mathcal{N} = 1$  TSC, it is important that we find a 2D HM with a single Fermi pocket, as we have in Eq.(2). That way, the HM / SC proximity effect we discussed will give us an equivalent of the single-spin  $p_x + ip_y$  SC with a single Fermi pocket

We find through band calculation 2D HMs with a single Fermi pocket, which is the main requirement for our model. One candidate we find is the  $\text{CrO}_2$  film that is two atomic layers thick in the (001) direction. Half-metallicity of bulk  $\text{CrO}_2$  has been confirmed by experiments, *e.g.* Refs.<sup>22,25</sup>. It was also experimentally shown to have a strong proximity effect to an  $s$ -wave SC -  $\text{NbTiN}$  - that has a relatively high  $T_c$  ( $\sim 14\text{K}$ ) and a spin-orbit coupling larger than the SC gap. Since the width of bands near Fermi level for  $\text{NbN}$  is about  $7.2\text{eV}$ <sup>26</sup> and the

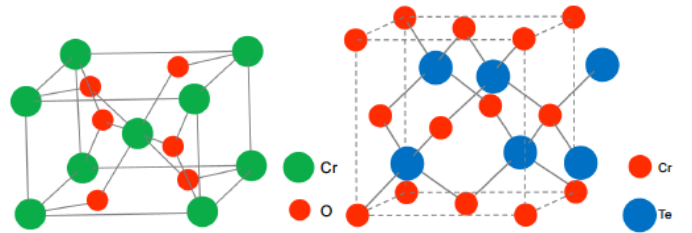


FIG. 3. Crystal structures of two candidate materials,  $\text{CrO}_2$  and  $\text{CrTe}$ . The left shows the rutile crystal structure of bulk  $\text{CrO}_2$ . The lattice constants are  $a = 0.4421\text{nm}$  and  $c = 0.2916\text{nm}$ . The distance between the nearest O and Cr on the same layer is  $0.1817\text{nm}$  and the nearest O and Cr on the adjacent layer is  $0.1929\text{nm}$ . The right shows the zinc blende crystal structure of bulk  $\text{CrTe}$ . Here, both Cr and Te forms body-centered cubic with the lattice constant of  $a = 0.6202\text{nm}$ . The zinc blende VTe has the same structure as the zinc blend  $\text{CrTe}$ , but with a slightly different lattice constant ( $0.6271\text{nm}$ ).

atomic spin-orbit coupling of Nb is  $0.1\text{eV}$ <sup>27</sup>, the mechanism discussed here may be able to induce a pairing gap up to  $\sim 1\text{K}$ . The bulk  $\text{CrO}_2$  crystal, as shown in Fig. 3, has a rutile structure, where the Cr atoms form body-centered tetragonal lattice and are surrounded by distorted O octahedra<sup>28</sup>. The lattice is compressed in the  $c$ -axis direction ( $c/a = 0.66$ ), with the lattice constant  $a = 0.44\text{nm}$ . Presence of a substrate is required if we are to maintain this rutile structure for a very thin  $\text{CrO}_2$  film, specifically a rutile oxide substrate with a good lattice matching. Another condition we need for the substrate is large insulating gap, since we do not want the substrate to affect the band structure of  $\text{CrO}_2$ . We find that the rutile oxide  $\text{TiO}_2$ , which has a  $3.0\text{eV}$  energy gap, is best suited for this purpose. As shown in Fig. 4 the band calculation for this  $\text{CrO}_2$ - $\text{TiO}_2$ (001) heterostructure (see Appendix B for details) shows that we obtain a HM with a single Fermi surface for a Fermi level range of  $\sim 0.2\text{eV}$ . This means that we do not require fine-tuning of the HM Fermi level, unlike in many of the previous proposals for obtaining the  $\mathcal{N} = 1$  TSC<sup>10</sup>.

Another candidate material for a 2D HM with a single Fermi surface is the zinc blende  $\text{CrTe}$  or VTe that is two atomic layers thick in the (111) direction. Both  $\text{CrTe}$  and VTe in the zinc blende structure have been shown to be half-metallic in the band calculation<sup>29</sup>; a thin film of the zinc blende  $\text{CrTe}$  has been fabricated in thin films by molecular-beam epitaxy<sup>30</sup>. As we see in Fig. 4, two atomic layers of zinc blende VTe (111) with the zinc blende  $\text{ZnTe}$  substrate (which has both an energy gap of  $2.3\text{eV}$  and a good lattice matching with the zinc blende  $\text{CrTe}$  or VTe) can have a single Fermi surface for the Fermi level range of  $0.3\text{eV}$  (see Appendix B for details). For  $\text{CrTe}$ , we find a slightly narrower Fermi level range for a single Fermi surface ( $\approx 0.06\text{eV}$ ).

*Detection:* Detecting the chiral Majorana edge state along with the fully gapped quasiparticle spectrum in the

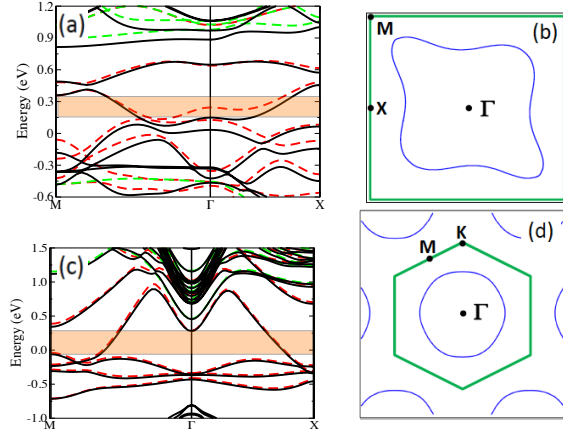


FIG. 4. (a) The band structure of the  $\text{CrO}_2\text{-TiO}_2(001)$  model. There is no spin degeneracy in these bands; the red and the green dotted curve shows the spin-up and -down bands when SOC is absent. The region shaded in orange shows the energy range, where we obtain a single Fermi pocket. (b) The single Fermi surface at energy level 0.15eV for  $\text{CrO}_2\text{-TiO}_2(001)$  model. The green box shows the first Brillouin zone(BZ). (c) The band structure of  $\text{ZnTe-VTe}(111)$  model, done in the same way as the  $\text{CrO}_2\text{-TiO}_2(001)$  model. (d) The single Fermi surface at energy level 0.25eV for  $\text{ZnTe-VTe}(111)$  model (the green box shows the first BZ).

bulk of the HM will confirm that we have  $\mathcal{N} = 1$  TSC in the HM. The most direct tool for detection would be measuring with STM the tunneling  $dI/dV$  vs.  $V$  spectra of the HM; indeed this method has been used recently to detect the SC proximity effect in a HM<sup>18</sup>. If  $p_x + ip_y$  pairing is induced,  $dI/dV$  is suppressed below  $V = |\Delta^{HM}|/e$  in the bulk while along the edge we will see the zero bias conductance peak. Another place to look for the zero bias conductance peak is the HM domain boundary. This is because this domain boundary will also be the boundary between  $p_x + ip_y$  and  $p_x - ip_y$  region in the SC state and there will be a chiral Majorana state running along this boundary.

In summary, we have shown that we can obtain the  $\mathcal{N} = 1$  TSC in a HM through proximity effect with an  $s$ -wave SC. In a model where the HM is coupled to the SC through hopping, the symmetry of SC pairing induced in the HM is determined entirely by the hopping term. Due to the interface Rashba spin-orbit coupling, the hopping term will induce the pairing with  $p + ip$  symmetry. In order for this  $p_x + ip_y$  pairing to lead to the  $\mathcal{N} = 1$  TSC, we need to have a HM with single Fermi surface, and our band calculation shows that this can be obtained for a very thin  $\text{CrO}_2$  film. STM measurement can be used to verify that TSC is induced in the HM.

We would like to thank Mac Beasley, Steve Kivelson, and Srinivas Raghu for sharing their insights. This work is supported by DOE under contract DE-AC02-76SF00515 (SBC), the Sloan Foundation (XLQ) and NSF under grant number DMR-0904264.

---

<sup>1</sup> F. Wilczek, *Nature Phys.* **5**, 614 (2009).  
<sup>2</sup> G. E. Volovik, *Sov. Phys. JETP* **67**, 1804 (1988).  
<sup>3</sup> N. Read and D. Green, *Phys. Rev. B* **61**, 10267 (2000).  
<sup>4</sup> R. Jackiw and P. Rossi, *Nucl. Phys. B* **190**, 681 (1981).  
<sup>5</sup> G. E. Volovik, *JETP Lett.* **70**, 609 (1999).  
<sup>6</sup> C. Nayak *et al.*, *Rev. Mod. Phys.* **80**, 1083 (2008).  
<sup>7</sup> A. P. Mackenzie and Y. Maeno, *Rev. Mod. Phys.* **75**, 657 (2003).  
<sup>8</sup> P. G. Bjornsson, Y. Maeno, M. E. Huber, and K. A. Moler, *Phys. Rev. B* **72**, 012504 (2005); J. Kirtley *et al.*, *ibid.* **76**, 014526 (2007).  
<sup>9</sup> L. Fu and C. L. Kane, *Phys. Rev. Lett.* **100**, 096407 (2008).  
<sup>10</sup> J. D. Sau, R. M. Lutchyn, S. Tewari, and S. Das Sarma, *Phys. Rev. Lett.* **104**, 040502 (2010).  
<sup>11</sup> X.-L. Qi, T. L. Hughes, and S.-C. Zhang, arXiv:1003.5448.  
<sup>12</sup> R. M. Lutchyn, J. D. Sau, and S. Das Sarma, *Phys. Rev. Lett.* **105**, 077001 (2010).  
<sup>13</sup> J. Alicea, *Phys. Rev. B* **81**, 125318 (2010).  
<sup>14</sup> R. A. de Groot, F. M. Mueller, P. G. van Engen, and K. H. J. Buschow, *Phys. Rev. Lett.* **50**, 2024 (1983).  
<sup>15</sup> L. P. Gorkov and E. I. Rashba, *Phys. Rev. Lett.* **87**, 037004 (2001); V. M. Edelstein, *Phys. Rev. B* **67**, 020505 (2003).  
<sup>16</sup> M. Eschrig, J. Kopu, J. C. Cuevas, and G. Schön, *Phys. Rev. Lett.* **90**, 137003 (2003).  
<sup>17</sup> R. S. Keizer *et al.*, *Nature* **439**, 825 (2006).  
<sup>18</sup> Y. Kalcheim *et al.*, arXiv:1010.0390.  
<sup>19</sup> G. Deutscher, *Rev. Mod. Phys.* **77**, 109 (2005).  
<sup>20</sup> Although this gap can be modified by electron-electron interaction in the HM<sup>31</sup>, comparison between the HM  $\text{CrO}_2$  specific heat obtained from band calculation<sup>32</sup> and experiment<sup>33</sup> indicates interaction effect can be small in HM.  
<sup>21</sup> W. E. Pickett, *Phys. Rev. Lett.* **77**, 3185 (1996).  
<sup>22</sup> Y. S. Dedkov *et al.*, *Appl. Phys. Lett.* **80**, 4181 (2002).  
<sup>23</sup> S. Raghu, A. Kapitulnik, and S. Kivelson, *Phys. Rev. Lett.* **105**, 136401 (2010).  
<sup>24</sup> X.-L. Qi, T. L. Hughes, and S.-C. Zhang, *Phys. Rev. B* **81**, 134508 (2010).  
<sup>25</sup> R. J. Soulen Jr. *et al.*, *Science* **282**, 85 (1998).  
<sup>26</sup> L. F. Mattheiss, *Phys. Rev. B* **5**, 315 (1972).  
<sup>27</sup> D. J. Machin and J. F. Sullivan, *J. Less Common Met.* **19**, 405 (1969).  
<sup>28</sup> M. A. Korotin, V. I. Anisimov, D. I. Khomskii, and G. A. Sawatzky, *Phys. Rev. Lett.* **80**, 4305 (1998).  
<sup>29</sup> W.-H. Xie, Y.-Q. Xu, B.-G. Liu, and D. G. Pettifor, *Phys. Rev. Lett.* **91**, 037204 (2003).  
<sup>30</sup> M. G. Sreenivasan, J. F. Bi, K. L. Teo, and T. Liew, *J. Appl. Phys.* **103**, 043908 (2008).  
<sup>31</sup> P. G. de Gennes, *Rev. Mod. Phys.* **36**, 225 (1964).  
<sup>32</sup> I. I. Mazin, D. J. Singh, and C. Ambrosch-Draxl, *J. Appl. Phys.* **85**, 6220 (1999).  
<sup>33</sup> H. Liu *et al.*, *Phys. Status Solidi (a)* **202**, 144 (2005).

## Appendix A: HM pairing correlation

Our model Hamiltonian can be solved exactly, as it is quadratic:

$$\begin{aligned} \mathcal{H} = & \text{const.} + \sum_{\mathbf{k}} (\epsilon_{\mathbf{k}} - \mu) f_{\mathbf{k}\uparrow}^\dagger f_{\mathbf{k}\uparrow} + \sum_{\mathbf{k}\sigma} E_{\mathbf{k}} \gamma_{\mathbf{k}\sigma}^\dagger \gamma_{\mathbf{k}\sigma} \\ & + \sum_{\mathbf{k}} [f_{\mathbf{k}\uparrow}^\dagger \{t_{\mathbf{k},\uparrow\uparrow} (u_{\mathbf{k}}^* \gamma_{\mathbf{k}\uparrow} + v_{\mathbf{k}} \gamma_{-\mathbf{k}\downarrow}^\dagger) \\ & + t_{\mathbf{k},\uparrow\downarrow} (u_{\mathbf{k}}^* \gamma_{\mathbf{k}\downarrow} - v_{\mathbf{k}} \gamma_{-\mathbf{k}\uparrow}^\dagger)\} + \text{h.c.}] \\ = & \frac{1}{2} \sum_{\mathbf{k}} \Psi_{\mathbf{k}}^\dagger H_{\mathbf{k}}^{BdG} \Psi_{\mathbf{k}}, \end{aligned} \quad (\text{A1})$$

where  $\Psi = (f_{\mathbf{k}\uparrow}, f_{-\mathbf{k}\uparrow}^\dagger, \gamma_{\mathbf{k}\uparrow}, \gamma_{\mathbf{k}\downarrow}, \gamma_{-\mathbf{k}\uparrow}^\dagger, \gamma_{-\mathbf{k}\downarrow}^\dagger)^T$  and

$$H_{\mathbf{k}}^{BdG} = \begin{bmatrix} h^{HM} & T_{\mathbf{k}} \\ T_{\mathbf{k}}^\dagger & \Lambda_{BdG} \end{bmatrix}, \quad (\text{A2})$$

with  $h^{HM} = \tau^z (\epsilon_{\mathbf{k}} - \mu)$ ,  $\Lambda_{BdG} = \text{diag}(E_{\mathbf{k}}, E_{\mathbf{k}}, -E_{\mathbf{k}}, -E_{\mathbf{k}})$ , and

$$T_{\mathbf{k}} = \begin{bmatrix} u_{\mathbf{k}}^* t_{\mathbf{k},\uparrow\uparrow} & u_{\mathbf{k}}^* t_{\mathbf{k},\uparrow\downarrow} & -v_{\mathbf{k}} t_{\mathbf{k},\uparrow\uparrow} & v_{\mathbf{k}} t_{\mathbf{k},\uparrow\downarrow} \\ v_{\mathbf{k}}^* t_{-\mathbf{k},\uparrow\uparrow}^\dagger & -v_{\mathbf{k}}^* t_{-\mathbf{k},\uparrow\downarrow}^\dagger & -u_{\mathbf{k}} t_{-\mathbf{k},\uparrow\uparrow}^\dagger & -u_{\mathbf{k}} t_{-\mathbf{k},\uparrow\downarrow}^\dagger \end{bmatrix} \quad (\text{A3})$$

This Hermitian matrix can be diagonalized:  $U_{\mathbf{k}}^\dagger H_{\mathbf{k}}^{BdG} U_{\mathbf{k}} = \Lambda_{\mathbf{k}}$ , where  $\Lambda_{\mathbf{k}} = \text{diag}(\lambda_1, \dots, \lambda_6)$  and  $U_{\mathbf{k}}$  is a unitary matrix that becomes an identity matrix in the  $t_{\mathbf{k},\uparrow\sigma} \rightarrow 0$  limit. We can also define the basis  $\tilde{\Psi}_{\mathbf{k}} \equiv U_{\mathbf{k}}^\dagger \Psi_{\mathbf{k}} = (\tilde{f}_{\mathbf{k}\uparrow}, \tilde{f}_{-\mathbf{k}\uparrow}^\dagger, \tilde{\gamma}_{\mathbf{k}\uparrow}, \tilde{\gamma}_{\mathbf{k}\downarrow}, \tilde{\gamma}_{-\mathbf{k}\uparrow}^\dagger, \tilde{\gamma}_{-\mathbf{k}\downarrow}^\dagger)^T$  that diagonalize our BdG Hamiltonian.

We can obtain pairing correlator  $\langle f_{-\mathbf{k}\uparrow} f_{\mathbf{k}\uparrow} \rangle$  from this diagonalization. Since this diagonalization allows us to express the original operators in terms of operators of  $\tilde{\Psi}$ ,

$$\begin{aligned} f_{\mathbf{k}\uparrow} = & (U_{\mathbf{k}})_{11} \tilde{f}_{\mathbf{k}\uparrow} + (U_{\mathbf{k}})_{12} \tilde{f}_{-\mathbf{k}\uparrow}^\dagger + (U_{\mathbf{k}})_{13} \tilde{\gamma}_{\mathbf{k}\uparrow} \\ & + (U_{\mathbf{k}})_{14} \tilde{\gamma}_{\mathbf{k}\downarrow} + (U_{\mathbf{k}})_{15} \tilde{\gamma}_{-\mathbf{k}\uparrow}^\dagger + (U_{\mathbf{k}})_{16} \tilde{\gamma}_{-\mathbf{k}\downarrow}^\dagger \\ f_{-\mathbf{k}\uparrow}^\dagger = & (U_{\mathbf{k}})_{21} \tilde{f}_{\mathbf{k}\uparrow} + (U_{\mathbf{k}})_{22} \tilde{f}_{-\mathbf{k}\uparrow}^\dagger + (U_{\mathbf{k}})_{23} \tilde{\gamma}_{\mathbf{k}\uparrow} \\ & + (U_{\mathbf{k}})_{24} \tilde{\gamma}_{\mathbf{k}\downarrow} + (U_{\mathbf{k}})_{25} \tilde{\gamma}_{-\mathbf{k}\uparrow}^\dagger + (U_{\mathbf{k}})_{26} \tilde{\gamma}_{-\mathbf{k}\downarrow}^\dagger, \end{aligned} \quad (\text{A4})$$

we can express the pairing amplitude in terms of elements of  $U_{\mathbf{k}}$ :

$$\begin{aligned} \langle f_{-\mathbf{k}\uparrow} f_{\mathbf{k}\uparrow} \rangle = & (U_{\mathbf{k}})_{12} (U_{\mathbf{k}})_{22}^* + (U_{\mathbf{k}})_{15} (U_{\mathbf{k}})_{25}^* + (U_{\mathbf{k}})_{16} (U_{\mathbf{k}})_{26}^* \\ = & (U_{\mathbf{k}})_{21}^* (U_{\mathbf{k}})_{22} + (U_{\mathbf{k}})_{51}^* (U_{\mathbf{k}})_{52} + (U_{\mathbf{k}})_{61}^* (U_{\mathbf{k}})_{62}. \end{aligned} \quad (\text{A5})$$

Since the column vectors of  $U_{\mathbf{k}}$  are eigenvectors of  $H_{\mathbf{k}}^{BdG}$ , we can obtain the pairing amplitude by obtaining the eigenvectors of  $H_{\mathbf{k}}^{BdG}$ . In practice, both the weak and strong hopping limit enables us to use perturbation theory for calculating the pairing amplitude.

### 1. Weak hopping at the HM Fermi surface

Here, we assume  $|t_{\mathbf{k},\uparrow\sigma}| \ll |\Delta_{\mathbf{k}}|$ . At the HM Fermi surface, we need to apply the degenerate second order

perturbation theory since  $h^{HM} = 0$ . Therefore, we write down eigenvectors only up to terms linear in  $t_{\mathbf{k}\sigma}$ :

$$\mathbf{F}_{\mathbf{k}}^{(i)} = \begin{bmatrix} A^{(i)} \\ B^{(i)} \\ -[A^{(i)} u_{\mathbf{k}} t_{\mathbf{k},\uparrow\uparrow}^* + B^{(i)} v_{\mathbf{k}} t_{-\mathbf{k},\uparrow\downarrow}] / E_{\mathbf{k}} \\ -[A^{(i)} u_{\mathbf{k}} t_{\mathbf{k},\uparrow\downarrow}^* - B^{(i)} v_{\mathbf{k}} t_{-\mathbf{k},\uparrow\uparrow}] / E_{\mathbf{k}} \\ -[A^{(i)} u_{\mathbf{k}}^* t_{\mathbf{k},\uparrow\uparrow}^* + B^{(i)} u_{\mathbf{k}}^* t_{-\mathbf{k},\uparrow\downarrow}] / E_{\mathbf{k}} \\ +[A^{(i)} u_{\mathbf{k}}^* t_{\mathbf{k},\uparrow\downarrow}^* - B^{(i)} u_{\mathbf{k}}^* t_{-\mathbf{k},\uparrow\uparrow}] / E_{\mathbf{k}} \end{bmatrix}, \quad (\text{A6})$$

( $i = 1, 2$ ) where  $A^{(i)}, B^{(i)}$  are  $O(1)$ . In this regime, we have

$$\langle f_{-\mathbf{k}\uparrow} f_{\mathbf{k}\uparrow} \rangle \approx [B^{(1)}]^* B^{(2)} = [A^{(1)} B^{(1)}]^*. \quad (\text{A7})$$

Note that up to quadratic order in  $t_{\mathbf{k}\sigma}$ ,  $(A^{(i)}, B^{(i)})^T$  are effectively eigenvectors of

$$H_{eff} = \frac{1}{E_{\mathbf{k}}} (-\tau^z \zeta_{\mathbf{k}} - \tau^x \text{Re} \eta_{\mathbf{k}} + \tau^y \text{Im} \eta_{\mathbf{k}}), \quad (\text{A8})$$

when  $|t_{\mathbf{k},\uparrow\sigma}|^2 = |t_{-\mathbf{k},\uparrow\sigma}|^2$ . To justify this approximation we need

$$\frac{|t_{\mathbf{k},\uparrow\downarrow}|}{|t_{\mathbf{k},\uparrow\uparrow}|} \frac{|u_{\mathbf{k}} v_{\mathbf{k}}|}{||u_{\mathbf{k}}|^2 - |v_{\mathbf{k}}|^2} \gg \frac{|t_{\mathbf{k},\uparrow\downarrow}|}{|\Delta_{\mathbf{k}}|} \quad (\text{A9})$$

at the HM Fermi surface. Within this approximation we obtain

$$\langle f_{-\mathbf{k}\uparrow} f_{\mathbf{k}\uparrow} \rangle \approx \frac{1}{2} \frac{\eta_{\mathbf{k}}}{\sqrt{|\zeta_{\mathbf{k}}|^2 + |\eta_{\mathbf{k}}|^2}}. \quad (\text{A10})$$

We also note that the half-metal spectrum is now gapped, with the gap of  $\frac{\sqrt{|\eta_{\mathbf{k}}|^2 + |\zeta_{\mathbf{k}}|^2}}{E_{\mathbf{k}}}$ . However, it is clear that only the  $\eta_{\mathbf{k}}$  part is related to pairing, so we obtain

$$\Delta_{\mathbf{k}}^{HM} = \frac{\eta_{\mathbf{k}}}{E_{\mathbf{k}}}. \quad (\text{A11})$$

### 2. Strong hopping at the HM Fermi surface

In order to apply perturbation theory in this limit, we note that  $\Delta_{\mathbf{k}}/t_{\mathbf{k},\uparrow\uparrow}$  and  $t_{\mathbf{k},\uparrow\downarrow}/t_{\mathbf{k},\uparrow\uparrow}$  are small variables now. It is therefore convenient to rewrite  $H_{\mathbf{k}}^{BdG}$  in a new basis consisting of a spin down electron and a spin down hole in the  $s$ -wave SC and spin up electrons and holes in bonding and anti-bonding states over the HM and the  $s$ -wave SC. At the HM Fermi surface, this gives us

$$\tilde{H}_{\mathbf{k}}^{BdG} = U^\dagger H_{\mathbf{k}}^{BdG} U = \begin{bmatrix} \tilde{h}_{\mathbf{k}}^{tun} & (\tilde{T}_{\mathbf{k}}^{pair})^\dagger \\ \tilde{T}_{\mathbf{k}}^{pair} & \tilde{\Lambda}_{\mathbf{k}} \end{bmatrix},$$

where  $\tilde{\Lambda}_{\mathbf{k}} = \tau^z (|u_{\mathbf{k}}|^2 - |v_{\mathbf{k}}|^2) E_{\mathbf{k}}$ ,

$$\begin{aligned} \tilde{h}_{\mathbf{k}}^{tun} = & \text{diag}(t_{\mathbf{k},\uparrow\uparrow}, t_{-\mathbf{k},\uparrow\uparrow}, -t_{\mathbf{k},\uparrow\uparrow}, -t_{-\mathbf{k},\uparrow\uparrow}) \\ & + \frac{|u_{\mathbf{k}}|^2 - |v_{\mathbf{k}}|^2}{2} E_{\mathbf{k}} \begin{bmatrix} 1 & -1 & -1 & 1 \\ -1 & 1 & 1 & -1 \\ 1 & 1 & -1 & -1 \end{bmatrix}, \end{aligned} \quad (\text{A12})$$

$$\tilde{T}_{\mathbf{k}}^{pair} = \sqrt{2} \begin{bmatrix} t_{\mathbf{k},\uparrow\uparrow}^*/2 & u_{\mathbf{k}}^* v_{\mathbf{k}} E_{\mathbf{k}} & t_{\mathbf{k},\uparrow\downarrow}^*/2 & -u_{\mathbf{k}}^* v_{\mathbf{k}} E_{\mathbf{k}} \\ u_{\mathbf{k}} v_{\mathbf{k}}^* E_{\mathbf{k}} & -t_{\mathbf{k},\uparrow\downarrow}/2 & -u_{\mathbf{k}} v_{\mathbf{k}}^* E_{\mathbf{k}} & -t_{\mathbf{k},\uparrow\downarrow}/2 \end{bmatrix}, \quad (\text{A13})$$

and

$$U = \begin{bmatrix} \frac{1}{\sqrt{2}} & \frac{1}{\sqrt{2}} & \frac{1}{\sqrt{2}} & \frac{1}{\sqrt{2}} \\ \frac{u_{\mathbf{k}}}{\sqrt{2}} & -\frac{v_{\mathbf{k}}}{\sqrt{2}} & -\frac{u_{\mathbf{k}}^*}{\sqrt{2}} & \frac{v_{\mathbf{k}}^*}{\sqrt{2}} \\ \frac{u_{\mathbf{k}}^*}{\sqrt{2}} & \frac{v_{\mathbf{k}}}{\sqrt{2}} & \frac{u_{\mathbf{k}}}{\sqrt{2}} & -\frac{v_{\mathbf{k}}^*}{\sqrt{2}} \\ \frac{v_{\mathbf{k}}}{\sqrt{2}} & -\frac{v_{\mathbf{k}}^*}{\sqrt{2}} & u_{\mathbf{k}}^* & u_{\mathbf{k}} \end{bmatrix} \quad (\text{A14})$$

(note that chose a gauge so that  $t_{\mathbf{k},\uparrow\uparrow}$  is real positive).

Our strong-hopping mode in 2Dl gives us three spin-polarized bands. We can see this from examining the column vectors of  $U$ . Note that the first and third columns represents the electron in the spin-up bonding and anti-bonding bands respectively, the second and fourth columns represents the hole in the spin-up bonding and anti-bonding bands respectively, and the last two columns represents the electron and the hole in the spin-down band. For  $t_{\mathbf{k},\uparrow\uparrow} = t_{\mathbf{k},\downarrow\downarrow}$ , we have three pairs of a electron state and a hole state degenerate in energy - two pairs for spin-up and one pair for spin-down. Therefore, we can again apply degenerate second order perturbation theory with three sets of bases

$$\tilde{\mathbf{F}}_{\mathbf{k}}^{(i)} = \begin{bmatrix} A^{(i)} \\ B^{(i)} \\ -A^{(i)} \frac{|u_{\mathbf{k}}|^2 - |v_{\mathbf{k}}|^2}{4} \frac{E_{\mathbf{k}}}{t_{\mathbf{k},\uparrow\uparrow}} \\ B^{(i)} \frac{|u_{\mathbf{k}}|^2 - |v_{\mathbf{k}}|^2}{4} \frac{E_{\mathbf{k}}}{t_{\mathbf{k},\uparrow\uparrow}} \\ A^{(i)} \frac{1}{\sqrt{2}} \frac{t_{\mathbf{k},\uparrow\downarrow}^*}{t_{\mathbf{k},\uparrow\uparrow}} + B^{(i)} \sqrt{2} u_{\mathbf{k}}^* v_{\mathbf{k}} \frac{E_{\mathbf{k}}}{t_{\mathbf{k},\uparrow\uparrow}} \\ A^{(i)} \sqrt{2} u_{\mathbf{k}} v_{\mathbf{k}}^* \frac{E_{\mathbf{k}}}{t_{\mathbf{k},\uparrow\uparrow}} - B^{(i)} \frac{1}{\sqrt{2}} \frac{t_{\mathbf{k},\uparrow\downarrow}^*}{t_{\mathbf{k},\uparrow\uparrow}} \end{bmatrix}, \quad (\text{A15})$$

$$\tilde{\mathbf{G}}_{\mathbf{k}}^{(i)} = \begin{bmatrix} C^{(i)} \frac{|u_{\mathbf{k}}|^2 - |v_{\mathbf{k}}|^2}{4} \frac{E_{\mathbf{k}}}{t_{\mathbf{k},\uparrow\uparrow}} \\ -D^{(i)} \frac{|u_{\mathbf{k}}|^2 - |v_{\mathbf{k}}|^2}{4} \frac{E_{\mathbf{k}}}{t_{\mathbf{k},\uparrow\uparrow}} \\ C^{(i)} \\ D^{(i)} \\ -C^{(i)} \frac{1}{\sqrt{2}} \frac{t_{\mathbf{k},\uparrow\downarrow}^*}{t_{\mathbf{k},\uparrow\uparrow}} + D^{(i)} \sqrt{2} u_{\mathbf{k}}^* v_{\mathbf{k}} \frac{E_{\mathbf{k}}}{t_{\mathbf{k},\uparrow\uparrow}} \\ C^{(i)} \sqrt{2} u_{\mathbf{k}} v_{\mathbf{k}}^* \frac{E_{\mathbf{k}}}{t_{\mathbf{k},\uparrow\uparrow}} + D^{(i)} \frac{1}{\sqrt{2}} \frac{t_{\mathbf{k},\uparrow\downarrow}^*}{t_{\mathbf{k},\uparrow\uparrow}} \end{bmatrix}, \quad (\text{A16})$$

$$\tilde{\mathbf{K}}_{\mathbf{k}}^{(i)} = \begin{bmatrix} -X^{(i)} \frac{1}{\sqrt{2}} \frac{t_{\mathbf{k},\uparrow\downarrow}}{t_{\mathbf{k},\uparrow\uparrow}} - Y^{(i)} \sqrt{2} u_{\mathbf{k}}^* v_{\mathbf{k}} \frac{E_{\mathbf{k}}}{t_{\mathbf{k},\uparrow\uparrow}} \\ -X^{(i)} \sqrt{2} u_{\mathbf{k}} v_{\mathbf{k}}^* \frac{E_{\mathbf{k}}}{t_{\mathbf{k},\uparrow\uparrow}} + Y^{(i)} \frac{1}{\sqrt{2}} \frac{t_{\mathbf{k},\uparrow\downarrow}^*}{t_{\mathbf{k},\uparrow\uparrow}} \\ X^{(i)} \frac{1}{\sqrt{2}} \frac{t_{\mathbf{k},\uparrow\downarrow}}{t_{\mathbf{k},\uparrow\uparrow}} - Y^{(i)} \sqrt{2} u_{\mathbf{k}}^* v_{\mathbf{k}} \frac{E_{\mathbf{k}}}{t_{\mathbf{k},\uparrow\uparrow}} \\ -X^{(i)} \sqrt{2} u_{\mathbf{k}} v_{\mathbf{k}}^* \frac{E_{\mathbf{k}}}{t_{\mathbf{k},\uparrow\uparrow}} - Y^{(i)} \frac{1}{\sqrt{2}} \frac{t_{\mathbf{k},\uparrow\downarrow}^*}{t_{\mathbf{k},\uparrow\uparrow}} \\ X^{(i)} \\ Y^{(i)} \end{bmatrix}. \quad (\text{A17})$$

We can show from the effective Hamiltonians for the above three bases that the chirality of the spin-down pairs will be opposite to that of the two sets of spin-up pairs.

The effective Hamiltonians of  $\tilde{\mathbf{F}}_{\mathbf{k}}^{(i)}$  and  $\tilde{\mathbf{G}}_{\mathbf{k}}^{(i)}$  can be written

$$\begin{aligned} \tilde{H}_{eff,\uparrow}^{\pm} &\approx \frac{E_{\mathbf{k}}}{|t_{\mathbf{k},\uparrow\uparrow}|^2} (\tau^z \zeta_{\mathbf{k}} + \tau^x \text{Re}\eta_{\mathbf{k}} - \tau^y \text{Im}\eta_{\mathbf{k}}) \\ &\pm |t_{\mathbf{k},\uparrow\uparrow}| \left[ \frac{1}{2} \frac{|\Delta_{\mathbf{k}}|^2}{|t_{\mathbf{k},\uparrow\uparrow}|^2} + \frac{1}{2} \frac{|t_{\mathbf{k},\uparrow\downarrow}|^2}{|t_{\mathbf{k},\uparrow\uparrow}|^2} + \frac{1}{8} \frac{(\epsilon'_{\mathbf{k}} - \mu')^2}{|t_{\mathbf{k},\uparrow\uparrow}|^2} \right], \end{aligned} \quad (\text{A18})$$

while for  $\tilde{\mathbf{K}}_{\mathbf{k}}^{(i)}$ , the effective Hamiltonian is

$$\tilde{H}_{eff,\downarrow} \approx \frac{2E_{\mathbf{k}}}{|t_{\mathbf{k},\uparrow\uparrow}|^2} (\tau^z \zeta_{\mathbf{k}} - \tau^x \text{Re}\eta_{\mathbf{k}} - \tau^y \text{Im}\eta_{\mathbf{k}}). \quad (\text{A19})$$

Because the tunneling process required for pairing the spin-down pairs is the reverse of what is required for pairing the spin-up pairs, the chirality of the spin-down pairs is opposite of that of the spin-up pairs. Eqs.(A18) and (A19) show that the HM / SC heterostructure overall has the  $\mathcal{N} = 1$  TSC. We believe that this result should hold even in the case the SC is 3D.

These effective Hamiltonian tells us that we have giving us

$$\Delta_{\mathbf{k}}^{HM} \approx \frac{\eta_{\mathbf{k}}}{|t_{\mathbf{k},\uparrow\uparrow}|^2} \Delta_{\mathbf{k}}, \quad (\text{A20})$$

since only the spin-up pairs involve the HM.

## Appendix B: 2D half-metal heterostructures

Here, we clarify what crystal structure we used for band structure calculation of  $\text{CrO}_2$  and  $\text{CrTe} / \text{VTe}$  in the zinc blende structure. We first note here that while the rutile structure we showed in Fig.3 is the stable structure for  $\text{CrO}_2$ , the same is not true for  $\text{CrTe}$  or  $\text{VTe}$ . However, the zinc blende  $\text{CrTe}$  has been grown on the zinc blende  $\text{ZnTe}$  substrate.

We note that the rutile structure cannot be maintained in a very thin film without support from a substrate. Basically, for a heavier Cr atom to be in equilibrium, it needs all six adjacent O atoms, but in the two atomic layer (001) film, there are only four O atoms adjacent to every Cr atom. Because of this, the Cr atoms of the lower layer will be displaced toward the upper layer, while the Cr atoms of the upper layer will be displaced toward the lower layer. In fact, a two-atomic layer of the rutile  $\text{CrO}_2$  (001) will actually turn into a Cr layer sandwiched between two O layers.

We now explain the details of the  $\text{CrO}_2\text{-TiO}_2$  (001) heterostructure we used for the Fig.4 band calculation. In order to retain the rutile structure, it is necessary to grow  $\text{CrO}_2$  on the (001) side of the rutile oxide with a good matching lattice constant, and as we explained in the main text,  $\text{TiO}_2$  fits this condition very well, as well as having a large insulating gap. However, this is not sufficient for obtaining the half-metal with a single Fermi surface, one of the reason being that the Cr atoms of the

upper layer is still displaced downward from its equilibrium position in the perfect rutile structure. We find that when we have two atomic layers of  $\text{TiO}_2$  (001) on the top of the two atomic layers of  $\text{CrO}_2$  (001), the  $\text{CrO}_2$  layers are half-metallic with a single Fermi surface, with very little structural distortion.

To maintain the zinc blende structure of  $\text{CrTe}$  or  $\text{VTe}$ , we always need a zinc blende substrate with a good matching lattice constant. The zinc blende  $\text{ZnTe}$  not only has the lattice constant matching within 1% but also has been used experimentally in growing the zinc blende  $\text{CrTe}$ . For  $\text{CrTe}$  or  $\text{VTe}$ , growing either of them on the (111) side of the zinc blende  $\text{ZnTe}$  is sufficient in obtaining both half-metallicity with a single Fermi surface and

the two atomic layer zinc blende (111) structure with very little structural distortion. In our calculation, when we used a  $\text{ZnTe}$  of finite thickness, the dipole moment between  $\text{Zn}$  and  $\text{Te}$  atoms give rises to an electric field in our heterostructure. Since this effect decreases when we increased the thickness of the  $\text{ZnTe}$  layer, we expect the effect to go away for a sufficiently thick  $\text{ZnTe}$  layer. For our band calculation, we added an extra atomic layer of the hydrogen atoms - which gives a  $\text{VTe} - \text{ZnTe} - \text{H}$  heterostructure - solely for canceling out this artificial electric field. In Fig 4 (c) we have omitted the  $\text{H}$  band, which do not mix with any  $\text{VTe}$  band due to both the insulating gap and the thickness of the  $\text{ZnTe}$  layer.